Supplemental Information

Supplemental Figures

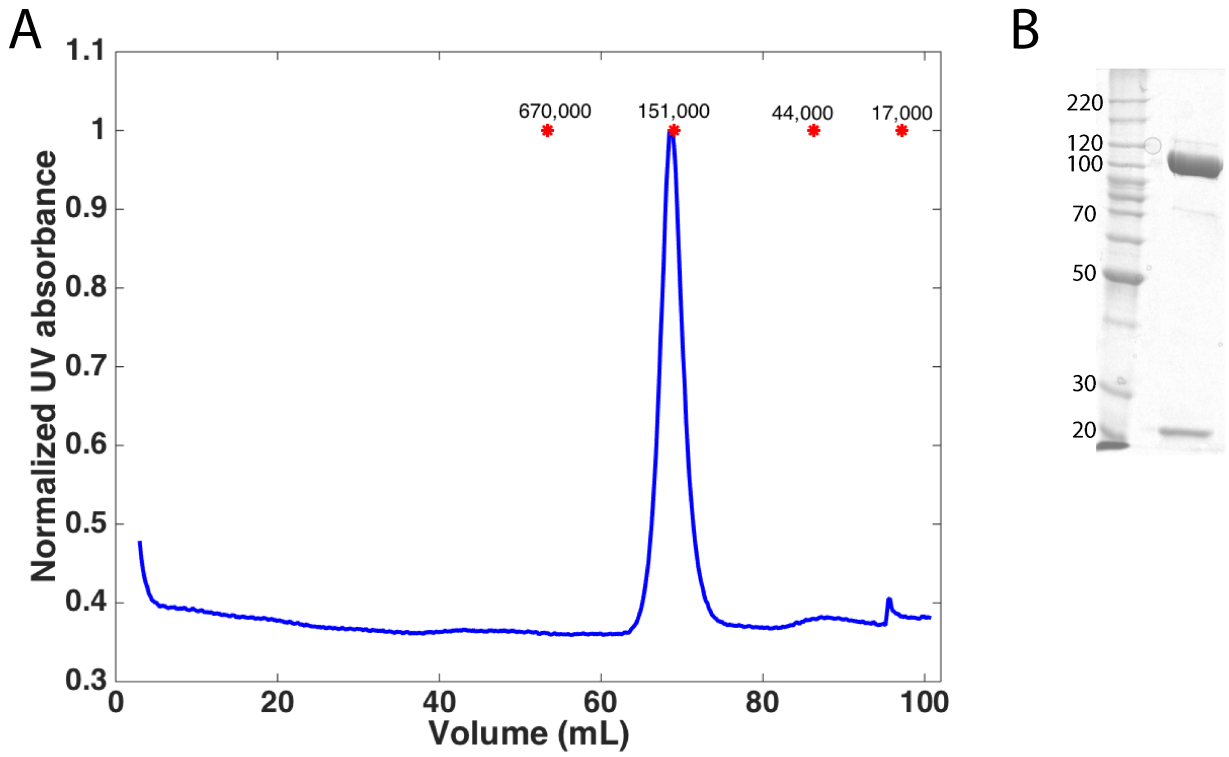

Figure S1. Related to Figures 2 and 3: (**a**) SEC chromatograph of purified sS1-eGFP myosin shows a single monomeric species eluting near its predicted molecular weight of ~145kD. The red asterisks show the migration positions of protein standards run on the Superdex 200 size exclusion column. (**b**). SDS-PAGE gel showing the purified sS1- eGFP myosin heavy chain (~120kD) and essential light chain (~25kD).

HCM mutation	Myosin	Velocity	ATPase	Force
R453C (Palmer et al., 2004)	Mouse α-cardiac	NC	0.6	-
R453C (Debold et al., 2007)	Mouse α-cardiac	NC	NC	1.8
R403Q (Debold et al., 2007)	Mouse α-cardiac	1.3	2.2	1.5
R403Q (Lowey et al., 2008)	Mouse α-cardiac	1.3	1.3	-
R403Q (Palmer et al., 2004)	Mouse α-cardiac	1.1	1.4	-
R403Q (Lowey et al., 2008)	Mouse β -cardiac	NC	NC	-
R403Q (Palmiter et al., 2000)	Human β-cardiac (human tissue)	1.3	-	-
R403Q (Belus et al., 2008)	Human β-cardiac (human tissue)	-	-	0.6
R453C (Sommese et al., 2013)	Human β-cardiac sS1	0.8	0.7	1.5
R403Q (Nag et al., 2015)	Human β-cardiac sS1	1.1	1.2	0.8
R719W (Kawana et al. dx.doi.org/10.1101/065649)	Human β-cardiac sS1	1.1	NC	0.8
R723G (Kawana et al. dx.doi.org/10.1101/065649)	Human β-cardiac sS1	1.1	NC	0.7
G741R (Kawana et al. dx.doi.org/10.1101/065649)	Human β-cardiac sS1	NC	NC	NC
H251N (this manuscript)	Human β-cardiac sS1	**1.4**	**1.3**	**1.5**
D239N (this manuscript)	Human β-cardiac sS1	**1.9**	**1.5**	**1.2**

Table S1. Related to Figures 2 and 3. Biomechanical parameters for myosins/myosin subfragments carrying various HCM mutations relative to WT myosin of the corresponding species. NC = no change. (-) = No data reported.

Myosin	Velocity (nm/s)	k_{cat} (s^{-1})	K_M (μm)	Intrinsic Force (pN)	S1-S2 K_D (μm)
WT	860 ± 10	4.5 ± 0.4	58 ± 9	1.3 ± 0.1	45 ± 10
H251N	1200 ± 20	5.6 ± 0.4	60 ± 10	1.9 ± 0.2	200 ± 30
D239N	1670 ± 40	6.7 ± 0.5	61 ± 10	1.6 ± 0.1	60 ± 8

Table S2. Related to Figures 2 and 3. Biomechanical parameters for WT and mutant sS1s. Actin gliding velocity was measured using the in vitro motility assay, k_{cat} and K_M were measured using an ATPase assay, and single molecule intrinsic force using optical tweezers. The error reported is the standard error of the mean.

Supplemental Methods

Expression and purification of recombinant human sS1 β-cardiac myosin

Recombinant human β-cardiac sS1 containing HCM causing mutations were co-expressed with a FLAG-tagged human ventricular cardiac essential light chain (ELC) in C2C12 mouse myoblast cells using adenoviral vectors, and purified using FLAG affinity and ion exchange chromatography as described (Sommese et al., 2013). The myosin construct includes either a C-terminal 8 amino acid peptide (RGSIDTWV), which acts as an affinity clamp (AC) that binds the PDZ-18 protein (sS1-AC), or a C-terminal eGFP, which binds to an anti-GFP antibody (sS1-eGFP).

C2C12 cells were grown at 37 °C and 8% CO_2 in growth medium (DMEM + 10% fetal bovine serum + 1x pen-strep). 10 plates of confluent C2C12 cells were differentiated to myotubes by replacing the growth medium with differentiation medium (DMEM + 2% horse serum + 1x pen-strep). The cells were differentiated for 2 days. Next, the cells were infected with adenoviruses carrying the myosin sS1 and FLAG-ELC in growth media ½ (DMEM + 5% fetal bovine serum + 1x pen-strep). The cells were infected for 4 days and then harvested. The media was removed from the cells, and they were washed with ice cold PBS. Then 1 ml of lysis buffer (20 mM imidazole pH7.5, 100 mM NaCl, 4 mM $MgCl_2$, 1 mM EGTA, 1 mM EDTA, 0.5% tween-20, 1 mM DTT, 3 mM ATP, 1 mM PMSF, 10% sucrose and Roche protease inhibitors) was added to each plate and the cells were harvested by scraping. The cells were lysed using a dounce homogenizer, and then centrifuged at 23000 rpm for 20 minutes using a Ti60 ultracentrifuge rotor. The supernatant was then incubated with 1mL of anti-FLAG resin for 2 hours at 4 °C. This allowed the sS1-ELC complex to bind to the resin. The resin was then gently spun at 2000 rpm for 2 min. The supernatant was discarded, and then the resin was washed with wash buffer (20 mM imidazole pH7.5, 150 mM NaCl, 5 mM $MgCl_2$, 1 mM EGTA, 1 mM EDTA, 1 mM DTT, 3 mM ATP, 1 mM PMSF, 10% sucrose and Roche protease inhibitors) and incubated in wash buffer overnight with TEV protease at 4°C to cleave off the FLAG-tag. The next day, the resin was spun and the supernatant containing the sS1was collected and further purified using anion exchange chromatography with a HiTrap-Q HP (Millipore) column. The purity of the protein was confirmed using SDS PAGE (**Figure S1**).

Actin activated ATPase assay

Only freshly prepared sS1-eGFP was used for this assay. Once the sS1 was purified, it was buffer exchanged into ATPase buffer (10 mM imidazole pH7.5, 5 mM KCl, 1 mM DTT, 3 mM $MgCl_2$) using amicon ultracell 10K filters. sS1concentration was measured using eGFP absorbance. To prepare F-actin, G-actin was dialyzed extensively into ATPase buffer to remove any residual ATP. Actin concentration was then measured using absorbance at 290 nm in a spectrophotometer. The steady-state actin-activated ATPase activities of the WT and mutant human β-cardiac sS1s were determined using a colorimetric assay to measure inorganic phosphate production at various time points (0 – 30 mins) from a solution containing sS1 (0.01mg ml^{-1}), ATP and increasing amounts of actin filaments (0 – 100 μM) (Trybus, 2000). All measurements were made at 23 °C. The time dependent rate for each actin concentration was calculated by fitting the phosphate signal as a function of time to a linear function. The slope was then converted to activity units normalized to a single myosin head. Kinetic parameters (i.e. k_{cat}) were extracted from the data by fitting the activity at each actin concentration to the Michaelis-Menten equation to determine maximal activity using the curve fitting toolbox in MatLab (De La Cruz and Ostap, 2009). The errors in the fitted values were determined using 100 bootstrap iterations.

In vitro motility assay

To remove myosin motors that bind actin irreversibly (dead heads), purified motor preparations were incubated with excess bovine skeletal actin on ice in the presence of ATP, then pelleted by ultracentrifugation (TLA 100; 95,000 rpm) at 4°C just prior to performing the assay.

For performing the assay, flow chambers were constructed using nitrocellulose cover slips attached to a glass slide using double sided tape. First PDZ-18 (4 μM) was added to the chamber and incubated for 2 minutes. Then the excess PDZ-18 was washed with 1mg ml^{-1} BSA (in 1x assay buffer). This also passivated the surface, which prevents non-specific sticking of sS1 and actin to the surface. Next, sS1-AC (0.2-0.4 μM) was added to the chamber,

and attached to the surface via PDZ. After 1-5 nM bovine actin labeled with phalloidin-tetramethylrhodamine (TMR) was added, movement was initiated by addition of ATP in the presence of oxygen scavenging (0.4% glucose, 0.11 mg/ml glucose oxidase, and 0.018 mg/ml catalase) and ATP regeneration systems (1 mM phosphocreatine, 0.1 mg/mL creatine phosphokinase). Actin filaments were detected under the microscope and at least 4 movies of 30 seconds were recorded for each condition. The movies for WT and H251N were recorded at 1 frame per second (fps) and D239N at 2 fps using an ANDOR iXon EMCCD camera. The mean velocity (MVEL, as described in Aksel et al.) was calculated using the FAST software (Aksel et al., 2015). All measurements were made at 23°C.

Loaded in vitro motility assay

The loaded in vitro motility assay was performed in a manner similar to the in vitro motility assay, with utrophin being used as the load molecule. Previously, other actin binding proteins such as alpha-actinin (Greenberg and Moore, 2010) have been used for loaded motility assay. However, due to the large size of alpha-actinin compared to sS1, we used utrophin, a smaller member of the actin binding protein family that includes alpha-actinin (Aksel et al., 2015). The utrophin contains the same C-terminal affinity clamp peptide as the sS1 for specific attachment to the surface via PDZ.

For the assay, first PDZ-18 is flowed in the microfluidic chamber made with nitrocellulose coated coverslips. Excess PDZ-18 is washed with 1mg ml^{-1} BSA (in 1x assay buffer). A mixture of sS1 and utrophin is added to the chamber, where the sS1 concentration is kept constant, and the utrophin concentration ranges from 0 – 3.2 nM. Excess sS1/utrophin mixture is washed with BSA. Motility is monitored after the addition of actin, and at least 2 different fields of view are measured at each utrophin concentration for at least 30 seconds. The same experiment is repeated for the mutant sS1s, and the concentrations of the mutant sS1 and the WT myosin are kept the same to prevent any artifacts due to variability in sS1 concentration. The sS1 concentration is measured using the Bradford Assay.

The binding of the utrophin to actin prevents the motion of actin, thereby reducing the mean velocity. A higher concentration of utrophin leads to lower velocity, because the same numbers of myosin motors have to work against increasing resistance provided by the utrophin molecules. Previous work by Greenberg and Moore has described the effect of frictional load caused by alpha-actinin (Greenberg and Moore, 2010) on myosin motility by using alpha-actinin and actin interaction parameters to convert the alpha-actinin concentration to an effective frictional load. On the other hand, as described in detail in a previous publication from our lab (Aksel et al., 2015), we showed that the load effect on the velocity by utrophin is likely due to a different mechanism than assumed by earlier workers using alpha-actinin, and more work needs to be done with loaded motility assays to be certain fits of the data are with a particular model are justified and meaningful; thus, we believe it is presently difficult to extract more than semi-quantitative/qualitative conclusions of such data. Nonetheless, our Figure 3d clearly shows that, at each utrophin concentration, the actin gliding velocities of the mutant motors are higher than that of the WT motor, thereby reflecting a higher ensemble force of the mutant motors. Even though this assay does not give an absolute measurement of load, it does provide an independent measurement to confirm the increase in functionality due to the mutations.

Single molecule optical trap assay and analysis of force data

Details of the experimental setup and data analysis are described elsewhere (Nag et al., 2015; Sommese et al., 2013). Briefly, dead myosin motors were removed as described above. The experiments were performed at 23°C. Coverslips were sparsely coated with 1.6 μm-diameter silica beads (Bangs Laboratories, Inc.) then with nitrocellulose. In an experiment, anti-GFP antibody (Abcam) was first flowed into the chamber, followed by 1 mg ml^{-1} BSA (in 1x assay buffer) to wash and prevent non-specific sticking, then ~200 pM sS1-eGFP. After a wash with BSA, the final solution was flowed in consisting of 5 mM ATP, 1 uM TMR-phalloidin-labelled biotinylated actin (Cytoskeleton) filaments, the oxygen-scavenging and ATP regeneration systems (as for the in vitro motility system above), and 1 μm-diameter neutravidin-coated polystyrene beads (ThermoFisher). An actin filament was attached between two trapped, neutravidin-coated beads to form a "dumbbell", then lowered near a platform bead for potential interaction with sS1. A trap stiffness of ~0.15 pN/nm was used.

Representative plots of single molecule force traces for the three motor proteins are shown in Figure 3c. Such raw traces were used to generate force histograms as shown in Figure 3d. Force histograms of individual molecules were fitted to a double Gaussian function (Nag et al., 2015; Sommese et al., 2013). A single Gaussian function could not be used to fit the histograms due to the presence of a long tail which has previously been reported for various muscle myosins (Guilford et al., 1997; Molloy et al., 1995) including cardiac myosin (Nag et al., 2015; Sommese et al., 2013; Sugiura et al., 1998). If a single Gaussian fit were used, this long tail would skew the reported force values, thus we use a double Gaussian fit to extract the force of the majority of events. A broad force distribution can result from the heterogeneity in the orientation of myosin heads with respect to the actin filament or due to the presence of different conformations of myosin during force production (Guilford et al., 1997; Nag et al., 2015). The major peak from the double Gaussian fit yielded the force of an individual molecule. Mean force for each protein was calculated from averaging the forces of individual molecules.

It is important to check that the conclusion of altered force production of mutants in comparison to wild type can be validated by analyzing the force data by another method. Cumulative probability distribution analysis was used to compare the force of the different sS1s. This method of analysis takes all events into account, including those in the above-mentioned tail of the histogram, from all the molecules. The probability distribution starts from a value close to zero at the lowest measurable force to 1 at the maximum force. The function at any particular force value is calculated as the number of events less than or equal to that force value divided by the total number of events.

A final, first-order way to interpret the force data (and to reaffirm our conclusions) between mutants and WT is to examine the histogram of all events from all molecules of one protein, as shown in Figure 3d. Despite the broad distributions with a tail apparent in these histograms, we can see that the two mutant sS1s produce higher forces than WT.

Microscale thermophoresis for sS1-S2 binding affinity

To assess the binding affinity between the sS1 and S2 regions of myosin, and how the mutations affected this interaction, we used microscale thermophoresis (MST). To study this interaction, we used freshly prepared sS1-eGFP and unlabeled S2 (β-cardiac myosin amino acids 839-968). The proximal S2 construct includes the first 126 amino acids of S2 and it begins 4 residues before the end of S1. Due to the low affinity between sS1 and S2, the S2 was concentrated to >300 μM to get a binding curve. Both proteins were dialyzed into MST assay buffer (10 mM Imidazole pH7.5, 100 mM KCl, 1 mM EDTA, 2 mM $MgCl_2$, 1 mM DTT, 500 μM ADP and 0.05% tween). Before using them for the assay, both proteins were centrifuged at 100,000 rpm in a TLA 100 rotor for 20 min to remove any aggregates. For the assay, we used 16 serial dilutions of S2 starting at > 300 μM, with a 3-fold dilution for each subsequent sample. The sS1 was kept constant at 50 nM. The samples were loaded into NT.115 premium treated capillaries, and incubated at room temperature for 45 minutes in the dark. All MST data was recorded at 23 °C. The sS1-S2 interaction was followed by monitoring the eGFP fluorescence. A blue LED at 30% excitation power (BLUE filter; excitation 460-480 nm, emission 515-530 nm) and IR-Laser power at 60% was used. Data analysis was performed with software NTAffinityAnalysis (Nanotemper Technologies) where the binding isotherms were derived from the raw fluorescence data. The binding isotherms were then fitted using Matlab, with the Hill equation for cooperativity, to estimate an apparent dissociation constant (K_D), using a linear regression method. There were preparation-to-preparation differences in the binding affinity, and the WT K_D ranged between 35-50 μM; however, the relative differences between WT and mutant sS1s were constant.

Development of human β-cardiac myosin protein models

We developed human β-cardiac myosin S1 models based on known motor domain structural data to best represent the human β-cardiac myosin, as described in Homburger et al.(Homburger et al., 2016). In brief, we retrieved the protein sequences of human β-cardiac myosin and the human cardiac ventricular light chains from the UNIPROT database: myosin heavy chain motor domain (MYH7) - P12883, myosin essential light chain (MYL3) - P08590, and myosin regulatory light chain (MYL2) - P10916. We used a multi-template homology modeling approach to build the structural coordinates of MYH7 (residues 1-840), MYL3 (residues 1-195), MYL2 (residues 1-166) and S2 (residues 841-1280). We obtained the three dimensional structural model of S1 in the poststroke state by integrating the known structural data from solved crystal structures, as described (Homburger et al., 2016). Briefly, the templates used for the modeling of the poststroke structure were obtained from the human β-cardiac myosin motor domain solved by Winkelmann et al. (Winkelmann et al., 2015) (PDB ID code 4P7H, no nucleotide in the active

site), supplemented with the rigor structure from the squid myosin motor domain (Yang et al., 2007) (PDB ID code 3I5G, no nucleotide in the active site) to model the converter domain, lever arm, and light chains missing from the Winkelmann structure. Regions of the myosin motor domain missing from both of these structures (loop1, loop2) were each separately built using the ModLoop program (Fiser and Sali, 2003), and regions in the regulatory light chains that were not solved in the squid myosin crystal structure were independently modeled using the I-TASSER prediction (Yang et al., 2015) method, and they were used as individual templates. Sequence alignment between MYH7, MYL3, and MYL2 with their respective structural templates was obtained. The model of the poststroke structure was acquired using the MODELER package (Sali and Blundell, 1993). We used a multi template modeling method: A total of 100 models were obtained, and the best model was selected based on the discrete optimized protein energy score. The structural models were energy-minimized using SYBYL7.2 (Tripos, Inc.) to remove potential short contacts. The final 3D model of the poststroke structure was validated using RAMPAGE (Lovell et al., 2003), which provides a detailed check on the stereochemistry of the protein structure using the Ramachandran map. The S2 region is a long coiled-coil structure; hence we used the template from the Myosinome database. The structural model of homology-modeled sequestered heads of human β-cardiac S1 is based on the 3D-reconstructed structure of tarantula skeletal muscle myosin thick filaments by Alamo et al.(Alamo et al., 2008). Visualizations were performed using PyMOL version 1.7.4 (www.pymol.org).

Supplemental videos

Supplemental video 1. Related to Figure 3. In vitro motility of WT sS1 myosin. (30 frames, acquired at 1 fps, and sped up to 3 fps, image size = 80 x 80 μm^2)

Supplemental video 2. Related to Figure 3. In vitro motility of H251N sS1 myosin. (30 frames, acquired at 1 fps, and sped up to 3 fps, image size = 80 x 80 μm^2)

Supplemental video 3. Related to Figure 3. In vitro motility of D239N sS1 myosin. (30 frames, acquired at 2 fps, and sped up to 6 fps, image size = 80 x 80 μm^2)

Supplemental References

Aksel, T., Choe Yu, E., Sutton, S., Ruppel, K.M., and Spudich, J.A. (2015). Ensemble force changes that result from human cardiac myosin mutations and a small-molecule effector. Cell Rep *11*, 910-920.

Alamo, L., Wriggers, W., Pinto, A., Bartoli, F., Salazar, L., Zhao, F.Q., Craig, R., and Padron, R. (2008). Three-dimensional reconstruction of tarantula myosin filaments suggests how phosphorylation may regulate myosin activity. Journal of molecular biology *384*, 780-797.

Belus, A., Piroddi, N., Scellini, B., Tesi, C., D'Amati, G., Girolami, F., Yacoub, M., Cecchi, F., Olivotto, I., and Poggesi, C. (2008). The familial hypertrophic cardiomyopathy-associated myosin mutation R403Q accelerates tension generation and relaxation of human cardiac myofibrils. The Journal of physiology *586*, 3639-3644.

De La Cruz, E.M., and Ostap, E.M. (2009). Kinetic and equilibrium analysis of the myosin ATPase. Methods in enzymology *455*, 157-192.

Debold, E.P., Schmitt, J.P., Patlak, J.B., Beck, S.E., Moore, J.R., Seidman, J.G., Seidman, C., and Warshaw, D.M. (2007). Hypertrophic and dilated cardiomyopathy mutations differentially affect the molecular force generation of mouse alpha-cardiac myosin in the laser trap assay. American journal of physiology Heart and circulatory physiology *293*, H284-291.

Fiser, A., and Sali, A. (2003). ModLoop: automated modeling of loops in protein structures. Bioinformatics *19*, 2500-2501.

Greenberg, M.J., and Moore, J.R. (2010). The molecular basis of frictional loads in the in vitro motility assay with applications to the study of the loaded mechanochemistry of molecular motors. Cytoskeleton (Hoboken) *67*, 273-285.

Guilford, W.H., Dupuis, D.E., Kennedy, G., Wu, J., Patlak, J.B., and Warshaw, D.M. (1997). Smooth muscle and skeletal muscle myosins produce similar unitary forces and displacements in the laser trap. Biophysical journal *72*, 1006-1021.

Homburger, J.R., Green, E.M., Caleshu, C., Sunitha, M.S., Taylor, R.E., Ruppel, K.M., Metpally, R.P., Colan, S.D., Michels, M., Day, S.M*., et al.* (2016). Multidimensional structure-function relationships in human beta-cardiac myosin from population-scale genetic variation. Proceedings of the National Academy of Sciences of the United States of America *113*, 6701-6706.

Lovell, S.C., Davis, I.W., Arendall, W.B., 3rd, de Bakker, P.I., Word, J.M., Prisant, M.G., Richardson, J.S., and Richardson, D.C. (2003). Structure validation by Calpha geometry: phi,psi and Cbeta deviation. Proteins *50*, 437-450.

Lowey, S., Lesko, L.M., Rovner, A.S., Hodges, A.R., White, S.L., Low, R.B., Rincon, M., Gulick, J., and Robbins, J. (2008). Functional effects of the hypertrophic cardiomyopathy R403Q mutation are different in an alpha- or beta-myosin heavy chain backbone. The Journal of biological chemistry *283*, 20579-20589.

Molloy, J.E., Burns, J.E., Kendrick-Jones, J., Tregear, R.T., and White, D.C. (1995). Movement and force produced by a single myosin head. Nature *378*, 209-212.

Nag, S., Sommese, R.F., Ujfalusi, Z., Combs, A., Langer, S., Sutton, S., Leinwand, L.A., Geeves, M.A., Ruppel, K.M., and Spudich, J.A. (2015). Contractility parameters of human beta-cardiac myosin with the hypertrophic cardiomyopathy mutation R403Q show loss of motor function. Science advances *1*, e1500511.

Palmer, B.M., Fishbaugher, D.E., Schmitt, J.P., Wang, Y., Alpert, N.R., Seidman, C.E., Seidman, J.G., VanBuren, P., and Maughan, D.W. (2004). Differential cross-bridge kinetics of FHC myosin mutations R403Q and R453C in heterozygous mouse myocardium. American journal of physiology Heart and circulatory physiology *287*, H91-99.

Palmiter, K.A., Tyska, M.J., Haeberle, J.R., Alpert, N.R., Fananapazir, L., and Warshaw, D.M. (2000). R403Q and L908V mutant beta-cardiac myosin from patients with familial hypertrophic cardiomyopathy exhibit enhanced mechanical performance at the single molecule level. Journal of muscle research and cell motility *21*, 609-620.

Sali, A., and Blundell, T.L. (1993). Comparative protein modelling by satisfaction of spatial restraints. Journal of molecular biology *234*, 779-815.

Sommese, R.F., Sung, J., Nag, S., Sutton, S., Deacon, J.C., Choe, E., Leinwand, L.A., Ruppel, K., and Spudich, J.A. (2013). Molecular consequences of the R453C hypertrophic cardiomyopathy mutation on human beta-cardiac myosin motor function. Proceedings of the National Academy of Sciences of the United States of America *110*, 12607-12612.

Sugiura, S., Kobayakawa, N., Fujita, H., Yamashita, H., Momomura, S., Chaen, S.T., Omata, M., and Sugi, H. (1998). Comparison of unitary displacements and forces between 2 cardiac myosin isoforms by the optical trap technique - Molecular basis for cardiac adaptation. Circ Res *82*, 1029-1034.

Trybus, K.M. (2000). Biochemical studies of myosin. Methods *22*, 327-335. PMID: 11133239.

Winkelmann, D.A., Forgacs, E., Miller, M.T., and Stock, A.M. (2015). Structural basis for drug-induced allosteric changes to human beta-cardiac myosin motor activity. Nature communications *6*, 7974.
Yang, J., Yan, R., Roy, A., Xu, D., Poisson, J., and Zhang, Y. (2015). The I-TASSER Suite: protein structure and function prediction. Nature methods *12*, 7-8.
Yang, Y., Gourinath, S., Kovacs, M., Nyitray, L., Reutzel, R., Himmel, D.M., O'Neall-Hennessey, E., Reshetnikova, L., Szent-Gyorgyi, A.G., Brown, J.H.*, et al.* (2007). Rigor-like structures from muscle myosins reveal key mechanical elements in the transduction pathways of this allosteric motor. Structure *15*, 553-564.